

# An empirical study of automatic wildlife detection using drone thermal imaging and object detection

Miao Chang<sup>a</sup>, Tan Vuong<sup>a</sup>, Manas Palaparathi<sup>a</sup>, Lachlan Howell<sup>b</sup>, Alessio Bonti<sup>a</sup>,  
Mohamed Abdelrazek<sup>c</sup>, Duc Thanh Nguyen<sup>a,\*</sup>

<sup>a</sup>Deakin University,

School of Information Technology, Geelong VIC 3220, Australia

<sup>b</sup>Deakin University,

School of Life and Environmental Sciences, Geelong VIC 3220, Australia

<sup>c</sup>Deakin University,

Applied Artificial Intelligence Institute, Burwood VIC 3125, Australia

---

## Abstract

Artificial intelligence has the potential to make valuable contributions to wildlife management through cost-effective methods for the collection and interpretation of wildlife data. Recent advances in remotely piloted aircraft systems (RPAS or “drones”) and thermal imaging technology have created new approaches to collect wildlife data. These emerging technologies could provide promising alternatives to standard labourious field techniques as well as cover much larger areas. In this study, we conduct a comprehensive review and empirical study of drone-based wildlife detection. Specifically, we collect a realistic dataset of drone-derived wildlife thermal detections. Wildlife detections, including arboreal (for instance, koalas, *phascolarctos cinereus*) and ground dwelling species in our collected data are annotated via bounding boxes by experts. We then benchmark state-of-the-art object detection algorithms on our collected dataset. We use these experimental results to identify issues and discuss future directions in automatic animal monitoring using drones.

**Keywords:** Drone, wildlife detection, object detection, artificial intelligence

---

---

\*Corresponding Author

*Email addresses:* changmiao@deakin.edu.au (Miao Chang), vuongt@deakin.edu.au (Tan Vuong), m.palaparathi@deakin.edu.au (Manas Palaparathi), l.howell@deakin.edu.au (Lachlan Howell), a.bonti@deakin.edu.au (Alessio Bonti), mohamed.abdelrazek@deakin.edu.au (Mohamed Abdelrazek), duc.nguyen@deakin.edu.au (Duc Thanh Nguyen)

## 1. Introduction

Wildlife, ecosystem and habitat protection require monitoring of wildlife species where regular and reliable population assessments and census trends are necessary [1]. Conventional ground-based survey techniques are time-consuming and labour-intensive. Demand for automatic surveillance systems continues to grow, supported by emerging technologies that have greatly improved the power, accuracy and efficiency of ecological data collection.

Artificial intelligence (AI) research has been used to develop automated wildlife monitoring systems. For instance, research in audio signal processing and machine learning are used to detect and classify bird calls [2, 3, 4, 5]. Image recognition techniques are adopted to detect and identify animals from camera traps [6, 7, 8]. Computer vision methods are applied to recognise aquatic creatures captured by autonomous underwater vehicles [9, 10, 11, 12, 13]. Recently, drones equipped with cameras and automated detection technologies have been applied to wildlife monitoring [14, 15]. Drones offer many advantages including large-scale data collection, non-invasive and real-time monitoring, cloud storage, and fast playback [16]. In addition, thermal imaging devices when attached to drones, can provide further aid to detecting cryptic animals and distinguishing species from their surrounding environment in low-lighting conditions (e.g., night time) [17, 18].

While the increasing volume of wildlife data is useful to ecological studies, it raises a demand on effective methods to process and analyse large-scale datasets. Manual animal counting can be labour-intensive and prone to interpreter bias, resulting in less reliable estimates [19, 20]. For instance, without automated detection capabilities, aerial imagery is not perceived as a viable option for kangaroo monitoring in Australia due to the intensive effort required to process high-volume data [21]. Automatic counting, on the other hand, can quickly process large numbers of images through AI-based methods, reducing deviations, saving time and labour, and improving accuracy. Recent advances in computing hardware and resources have made AI algorithms feasible in many real-world applications.

A commonly adopted approach to automate the counting process is to apply ob-

ject detection algorithms [22, 23, 24], examples of AI-based methods, to find animal individuals from recorded aerial imagery. Object detection aims to localise instances of objects of interest, e.g., animals, and specify the semantic class, e.g., species, for each detection [25]. As shown in the literature [19, 21, 26, 27, 28], object detection has proven promise to enable automatic animal counting solutions, solving issues of laborious processing of large-scale wildlife datasets and aiding wildlife monitoring efforts. In addition, the availability of open-source object detectors has made object detection-based solutions feasible.

Given the rising uptake of drones and thermal imaging in automatic wildlife monitoring, we aim to conduct an empirical study of drone-based wildlife monitoring through object detection. Our work differs from other studies, e.g., [19, 20, 15, 27, 29], in several aspects. First, the novelty of our work relies on the empirical aspect of our review where we evaluated existing wildlife monitoring methods empirically, rather than just describing the methods as in other surveys, e.g., [15, 29]. Second, compared with [19, 20, 27], we benchmark more modern object detection techniques. Third, since we evaluate existing methods on the same dataset using the same settings, observations drawn from our experiments would be more conclusive. In summary, we make the following contributions in our work.

- A concise review of drone-based wildlife monitoring research since 2018 (Section 2);
- An annotated dataset of wildlife thermal detections captured using drones in forested environments (Section 3);
- Extensive experiments and benchmark results of many modern state-of-the-art object detection algorithms in detecting thermal signatures (Section 4).

## **2. Literature review**

### *2.1. Drone types and settings*

Depending on the species-specific or habitat-specific characteristics of the studied species, different settings can be applied to the drone. For instance, to collect koala

imagery, Winsen et al. [27] set the drone at an altitude of 60 m. This setting was subject to the height of the canopy and the terrain of the site, and therefore was adjusted to maintain a flight altitude about 30 m above the canopy. In [20], the flight altitude was set at 100 m to detect waterbird species and the drone captured images in a high resolution to minimise the long-distance temperature measurement error. Cox et al. [30] evaluated different drone thermal sensors for detecting rabbit burrows and suggested a minimum export rate of 30 Hz to ensure image quality.

Compared with ground surveys, drone-based surveys can collect wildlife data in severe conditions such as night time, winter, due to thermal sensors use. In several cases, both RGB and thermal information are combined to enhance animal detection [18]. We summarise technical parameters of common drone settings in Table 1.

## 2.2. *Animal detection*

After images are collected, object detection algorithms are used to detect animals. Animal detection aims to locate animal species in an input image. The task of animal detection has various challenges. Since drones acquire images from a high altitude, animal signatures become extremely small and many important characteristics (e.g., colour, texture, shape cannot be well captured). Animals also often blend into cluttered backgrounds (e.g., dense vegetation), making them indistinguishable from their surrounding environment.

Commonly used object detectors for animal detection from drone-based imagery include RetinaNet [22], Faster RCNN [23], and YOLO [24]. These detectors are network architectures divided into two branches to perform two sub-tasks: bounding box estimation (for object localisation) and bounding box classification (for object identification). When adapting these tools to animal detection, one needs to customise the last layer in the classification branch of the detector with new neurons corresponding to animal classes of interest, and then re-train the modified detector on an animal dataset. Some other older detectors such as SSD [33] and R-FCN [34] were used for bird detection in [20].

Several methods create their own model for animal detection. For instance, Wu et al. [16] proposed a depth density estimation network (based on ResNet [35]) to generate

Table 1: Summary of drone-based animal monitoring studies since 2018.

<b>Study (year)</b>	<b>Drone &amp; sensor</b>	<b>Image resolution</b>	<b>Object detector</b>
[31] (2018)	SenseFly eBee Canon PowerShot S110 (RGB)	4000 × 3000	CNN
[19] (2019)	Matrice 600 Pro FLIR Tau 2 (thermal)	640 × 512	Faster RCNN, YOLO
[20] (2019)	K-mapper NX-500 (RGB)	6480 × 4320	RetinaNet, SSD, R-FCN, Faster RCNN, YOLO
[18] (2021)	Matrice 210 FLIR Zenmuse XT2 (thermal, RGB)	640 × 512 (thermal) 4000 × 3000 (RGB)	Sobel detector
[21] (2021)	DJI Inspire-I RPA FLIR Zenmuse (thermal)	640 × 512	YOLO
	DJI Matrice 210 RPA FLIR Zenmuse XT 640 (thermal)	640 × 512	YOLO
[26] (2021)	DJI Phantom III 1/2.3" CMOS, effect. pixels: 12.4M (RGB)	4000 × 3000	SSD, YOLO
[27] (2021)	Matrice 600 Pro FLIR Tau 2 (thermal)	640 × 512	Faster RCNN, YOLO
[32] (2021)	DJI Matrice 600 Pro FLIR Tau 2 (thermal)	640 × 512	Faster RCNN, YOLO
[16] (2022)	Dahua ONVIF (RGB)	1024 × 768	Depth density network
[17] (2022)	Leica Aibot A X20 WIRIS Pro (thermal, RGB)	640 × 512 (thermal) 1920 × 1080 (RGB)	Image matching
[28] (2022)	DJI Inspire-II Zenmuse X7 (RGB)	6016 × 4008	RetinaNet
Ours (2023)	Mavic 2 Enterprise Advanced Uncooled VOx Microbolometer (thermal) 1/2" CMOS, effect. pixels: 48M (RGB)	640 × 512 (thermal) 3840 × 2160 (RGB)	RetinaNet, Faster RCNN, YOLO, FCOS, DDETR

a heat map of waterbirds density. Kellenberger et al. [31] and Barbedo et al. [36] divided an input image into a regular grid, on which a CNN was built to estimate the probability of having animals on every grid cell.

A common practice is to adopt a model pre-trained on large-scale datasets, e.g., ImageNet [37], COCO [38], then fine-tune it on a target domain [15]. Since each detector has its own advantages, to maximise the benefit brought by multiple detectors, one can combine different detectors via fusing their detection results [19, 32] or through ensemble learning [27]. Corcoran et al. [19] applied temporal information to perform animal tracking to remove false alarms. Ulhaq et al. [21] replaced the upsampling operators in the YOLO’s architecture with dilated convolutions to address feature corruption in the upsampling steps. Several strategies were proposed in [31] to handle class imbalance issue in training sets, including using class distribution in a training set to weight the loss function and cropping training images to reduce background bias.

Traditional image processing techniques also exist for animal detection. Lee et al. [18] applied the Sobel edge detector to extract edges from input images, then verified important edges using thermal information, requiring a lot of user-defined parameters. Mirka et al. [17] detected monkeys by matching moving objects between frames using ORB [39] (a handcrafted image descriptor like SIFT [40]). We present object detectors used in existing studies in Table 1.

### **3. Dataset**

#### *3.1. Field method and data collection*

We deployed a Mavic 2 Enterprise Advanced equipped with a  $640 \times 512$ -pixel thermal camera ( $\sim 9$  mm focal length), and a  $3840 \times 2160$ -pixel RGB camera (see Table 1). Both sensors worked at 30 Hz. The white-hot thermal pallet was used, and the thermal sensor was set to high gain.

We focused on developing a real-world dataset of all suspected wildlife thermal signatures detected in a given study area. We surveyed 25 ha plots of native forest in three locations in East Gippsland, Victoria, Australia, including two plots in Gelantipy ( $37^{\circ}13'31.65''S$ ,  $148^{\circ}15'34.34''E$  and  $37^{\circ}16'53.30''S$ ,  $148^{\circ}14'39.24''E$ ) and two plots

in Orbost (37°44'26.88"S, 148°12'15.21"E and 37°43'59.75"S, 148°12'16.41"E) across 17-20 May and 6-8 June 2022 in Gelantipy, and across 20-23 June 2022 in Orbost. Sites in Gelantipy consisted of Montane Grassy Woodland (composed of Broad-leaved peppermint, *Eucalyptus dives*, and Candlebark, *Eucalyptus rubida*) and Valley Grassy Forest (composed of River peppermint, *Eucalyptus elata*, Manna gum, *Eucalyptus viminalis*, White stringybark, *Eucalyptus globoidea*, Red box, *Eucalyptus polyanthemus*). Sites in Orbost consisted of Lowland forest with dominant tree species Silvertop Ash (*Eucalyptus sieberi*).

Minimum temperatures for the survey period ranged from 0.3–8°C, and maximum temperatures ranged from 6.1–18.4°C across the survey period. Wind speed was consistently <7.7 m/s. Surveys occurred between ~6pm–2am to maximise temperature differential and contrast between animals and the surrounding environment. Flights were programmed using UgCS 4.9.814 and were flown in a lawn mower pattern composed of parallel linear survey lines with 10% overlap. Flight altitude was 50-70 m above ground level depending on site-specific terrain and tree height. Flight speed was 5-6 m/s. Since the data were captured at night, only thermal images were retained and used in our experiments.

Surveys were conducted under Deakin University's Animal Ethics Committee Wildlife-Burwood protocol: B08-2022.

### 3.2. Data annotation

After collecting imagery data, we manually extracted images containing suspected thermal detections of wildlife species. We used CVAT<sup>1</sup>, a free and open-source annotation tool to label bounding boxes of suspected wildlife thermal signatures in the extracted images. During surveys in-field, we were only able to validate a small number of detected thermal signatures (64 signatures) using on-ground observers due to weather and other external factors. Due to a lack of thermal signature validation, we annotated only one class: "suspected wildlife signature". We note that this limitation does not compromise the aim of this empirical study, benchmarking available object

---

<sup>1</sup><https://cvat.org>

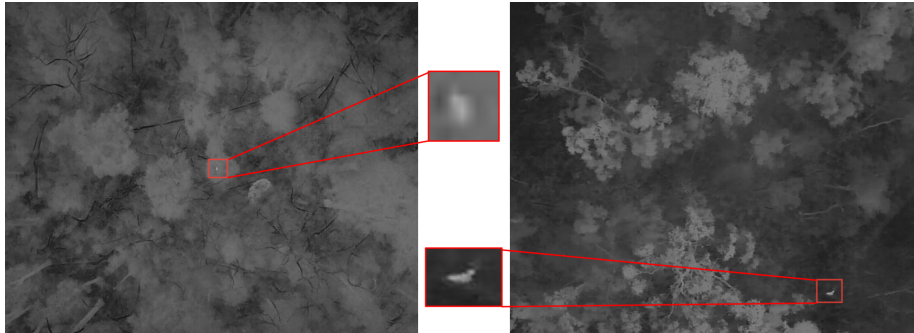


Figure 1: Illustration of annotated animals (with close-ups).

detection models on their detection accuracy and efficiency.

Annotated thermal signatures are very small ( $32 \times 32$  pixels relative to the image resolution of  $640 \times 512$  pixels). Annotation resulted in a dataset of 1,210 images with 1,814 annotated thermal signatures. We split the dataset into two subsets: training (850 images with 1,273 thermal signatures) and validation (360 images with 541 thermal signatures). We visualise several annotation results in Figure 1.

## 4. Benchmark of animal detection

### 4.1. Baselines

We experimented with the following object detection baselines: RetinaNet [22], Faster RCNN [23], YOLO [24], FCOS [41], and DDETR [42]. These were selected due to their high detection rate and fast computational speed, proven in many applications and on various datasets. RetinaNet, YOLO, and Faster RCNN make use of anchor boxes in finding object bounding boxes. In contrast, FCOS and DDETR are anchor box-free methods. DDETR is built based on Vision Transformer [43], a modern network architecture.

Some detectors have different variants. For instance, YOLO has a long history of development with many variants corresponding to different amendments in the architecture (for both feature learning and object location prediction) [44]. In this paper, we experimented with the versions 4, 5, and 7 of YOLO due to their contemporary as

well as proven superiority over other versions in the YOLO family [45, 46]. Moreover, YOLOv5 (the fifth version of YOLO) has also shown promise to detect objects in drone imagery [47, 45]. For YOLOv4, we evaluated the original version in [48, 49] and its variants, e.g., with the use of Cross Stage Partial connections [50] (csp), with different activation functions (mish, leaky), and network sizes (x: large, s: small). For YOLOv5, we experimented with 4 variants corresponding to 4 different scales (s: small, m: medium, x: large, and x: extra-large). For YOLOv7 [46], we benchmarked variants developed for different hardware specifications, e.g., edge GPU (YOLOv7-tiny), normal GPU (YOLOv7), cloud GPU (YOLOv7-w6), different sub-structures in the network architecture, e.g., YOLOv7-x, YOLOv7-e6e, YOLOv7-d6, and different backbones, e.g., YOLOv7-PRB, i.e., with the Parallel Residual Bi-Fusion (PRB) Feature Pyramid Network [51].

For Faster RCNN, we evaluated commonly used backbones including ResNet50, ResNet101 [35] and HRNet [52] (which is designed for high-resolution images). Both the ResNet50 and ResNet101 were also used and evaluated in RetinaNet. These variants have varying numbers of parameters, resulting in different training and inference speed. We summarise the object detectors experimented in our study in Table 2.

We adopted publicly released code repositories including Ultralytics<sup>2</sup> for YOLOv5, mmdetection<sup>3</sup> for RetinaNet, Faster RCNN, and FCOS, and the official implementation by the authors of YOLOv4<sup>4</sup>, YOLOv7<sup>5</sup>, YOLOv7-PRB<sup>6</sup>, and DDETR<sup>7</sup>.

#### 4.2. Experiments, results, and discussions

We implemented all the baselines in Pytorch 1.8.0 with Cuda 10.1. All experiments were conducted on 20 cores of Intel(R) Xeon(R) CPU E5-2630 v4@2.20GHz and 8 NVIDIA GeForce GTX 1080 Ti GPUs. Each model and its variants were trained using the same settings (see Table 3).

---

<sup>2</sup><https://github.com/ultralytics/yolov5>

<sup>3</sup><https://github.com/open-mmlab/mmdetection>

<sup>4</sup>[https://github.com/WongKinYiu/PyTorch\\_YOLOv4](https://github.com/WongKinYiu/PyTorch_YOLOv4)

<sup>5</sup><https://github.com/WongKinYiu/yolov7>

<sup>6</sup>[https://github.com/pingyang1117/PRBNet\\_PyTorch](https://github.com/pingyang1117/PRBNet_PyTorch)

<sup>7</sup><https://github.com/fundamentalvision/Deformable-DETR>

Table 2: Summary of object detection models regarding to Floating Point Operations Per Second - FLOPS (G), number of parameters (M), training time (hours:minutes), inference speed (frames per second - fps).

<b>Model</b>	<b>FLOPS ↓</b>	<b>No. Param ↓</b>	<b>Training time ↓</b>	<b>Inference speed ↑</b>
RetinaNet (ResNet50)	81.69	36.10	1h:32m	21.20
RetinaNet (ResNet101)	110.22	54.99	1h:55m	17.80
Faster RCNN (ResNet50)	78.12	41.12	1h:50m	18.70
Faster RCNN (ResNet101)	108.55	60.11	2h:55m	24.10
Faster RCNN (HRNet)	109.46	46.87	2h:00m	16.90
YOLOv4	107.10	63.94	1h:10m	19.90
YOLOv4-csp-s-leaky	16.40	8.06	0h:43m	13.20
YOLOv4-csp-leaky	107.50	52.50	0h:53m	18.20
YOLOv4-csp-x-leaky	184.40	99.22	1h:20m	21.90
YOLOv4-csp-s-mish	16.40	8.05	0h:30m	14.20
YOLOv4-csp-mish	107.50	52.50	0h:57m	18.40
YOLOv4-csp-x-mish	184.40	99.22	1h:45m	21.90
YOLOv5s	15.90	7.02	0h:21m	73.40
YOLOv5m	48.20	20.87	0h:28m	52.42
YOLOv5l	108.20	46.13	0h:45m	40.78
YOLOv5x	203.80	86.17	1h:22m	26.21
YOLOv7	105.10	37.20	1h:17m	11.90
YOLOv7-tiny	13.20	6.01	1h:00m	3.80
YOLOv7-w6	101.80	80.90	2h:36m	10.80
YOLOv7-x	188.90	70.82	5h:28m	13.10
YOLOv7-e6e	225.40	164.82	3h:25m	20.40
YOLOv7-d6	198.30	152.89	5h:48m	17.20
YOLOv7-PRB	255.30	102.15	1h:35m	25.20
FCOS	109.06	50.78	1h:20m	26.40
DDETR	27.40	39.82	2h:58m	16.20

Table 3: Experimental settings.

Model	Learning rate	Optimiser	Batch size	Epochs
RetinaNet	0.001	SGD	16	100
Faster RCNN	0.02	SGD	16	100
YOLOv4	0.01	SGD	8	100
YOLOv5	0.01	SGD	32	100
YOLOv7	0.01	SGD	4	100
FCOS	0.005	SGD	16	100
DDETR	0.0002	Adam	8	100

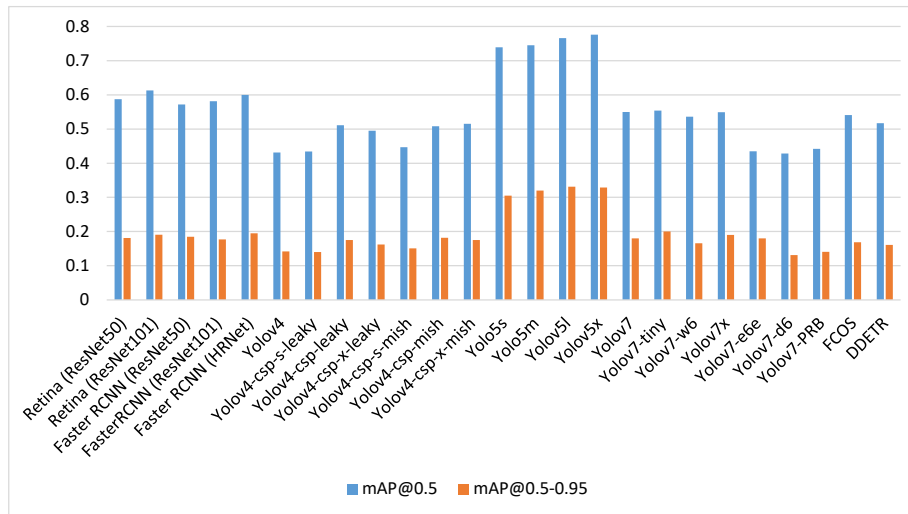


Figure 2: Detection accuracy of state-of-the-art baselines on our validation set.



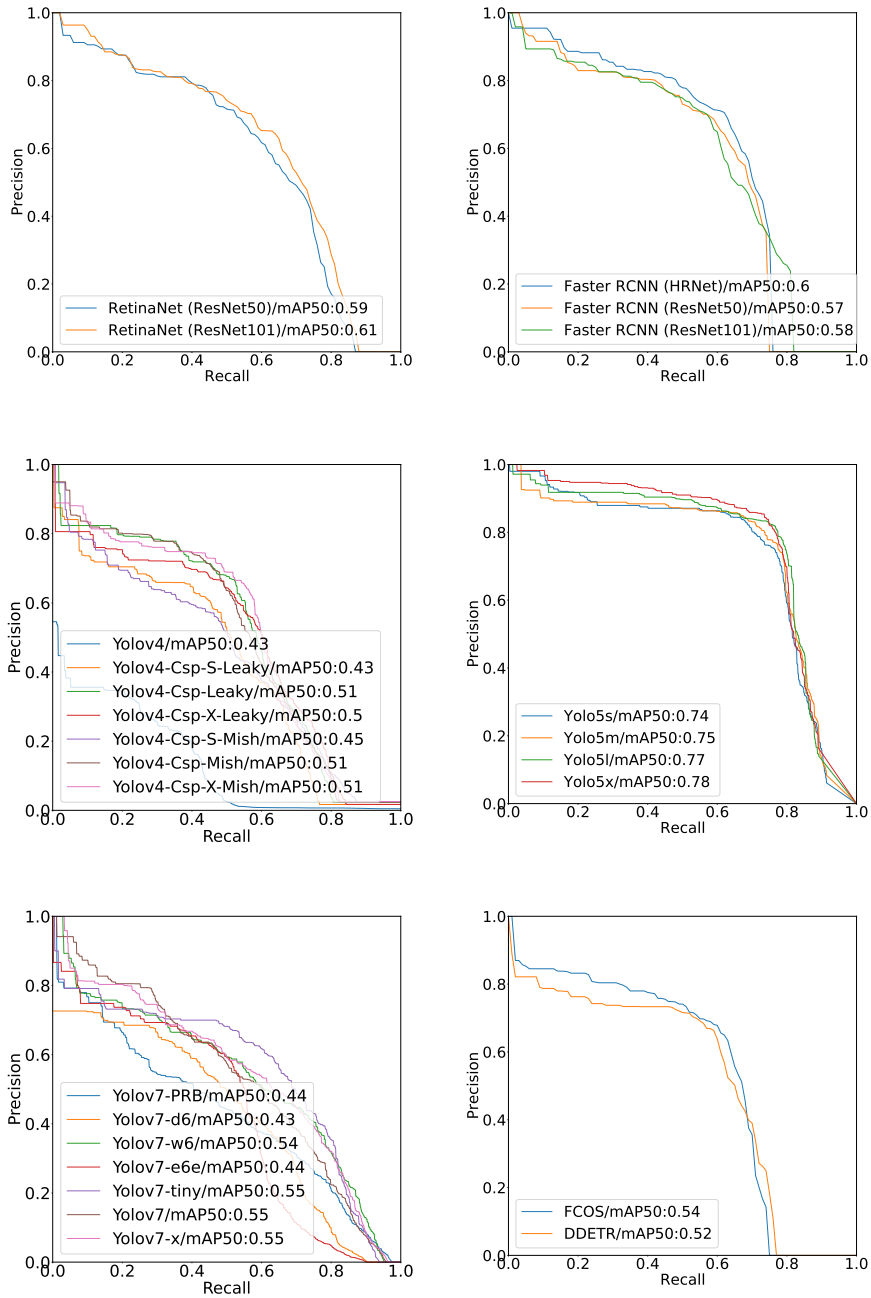


Figure 4: PR curves of the baselines on our validation set.

detection accuracy while both the baselines have comparable performance in terms of the inference speed. In general, all variants of the YOLO’s family clearly show the trade-off between model capacity and efficiency (i.e., larger models perform slower but get better accuracy). For instance, the tiny variant of YOLOv7 (YOLOv7-tiny) obtains the highest detection rate (0.55 mAP@0.5 and 0.20 mAP@0.5-0.95) among all the variants of the YOLOv7 baseline but also incurs the slowest speed (3.8 fps). Except for YOLOv7-tiny, both the YOLOv4’s and YOLOv7’s variants perform at around 10 to 25 fps.

The RetinaNet baseline ranks second overall and its best architecture (with highest detection accuracy) is ResNet101. However, the difference in the detection accuracy between the ResNet50 and ResNet101 backbones is marginal (about 0.02 mAP@0.5 and 0.01 mAP@0.5-0.95). This baseline also shows relatively slow inference speed (21.2 fps and 17.8 fps for the ResNet50 and ResNet101 backbones respectively).

The Faster RCNN baseline seems to take the third place although the difference in its range of detection rates compared with that of the RetinaNet baseline is negligible. In particular, the range of detection rates of the Faster RCNN detector is [0.572, 0.6] while it is [0.587, 0.613] for the RetinaNet detector. Experimental results also show that the combination of the Faster RCNN baseline with the HRNet backbone outperforms other variants made of the ResNet50 and ResNet101 backbones. This is probably due to the design of the HRNet backbone to deal with high-resolution images. Note that, as shown in Table 2, despite making use of less complex architecture (with less parameters and thus lower FLOPS), the Faster RCNN with the HRNet backbone takes longer inference time, compared with the RetinaNet with the ResNet101 backbone.

The two modern detectors, FCOS and DDETR, do not show advantages in our study. In addition, since those methods are anchor-free, they take time to learn bounding box locations but perform at the same speed (e.g., Faster RCNN) or slower than anchor-based baselines (e.g., YOLOv5).

To further investigate the learning process of the baselines, we plot the learning curves of all the baselines in Figure 5. We observed that all the baselines perform consistently on both the training and validation set. First, all the baselines show the convergence of their losses during the training, proving their learning ability. Second,

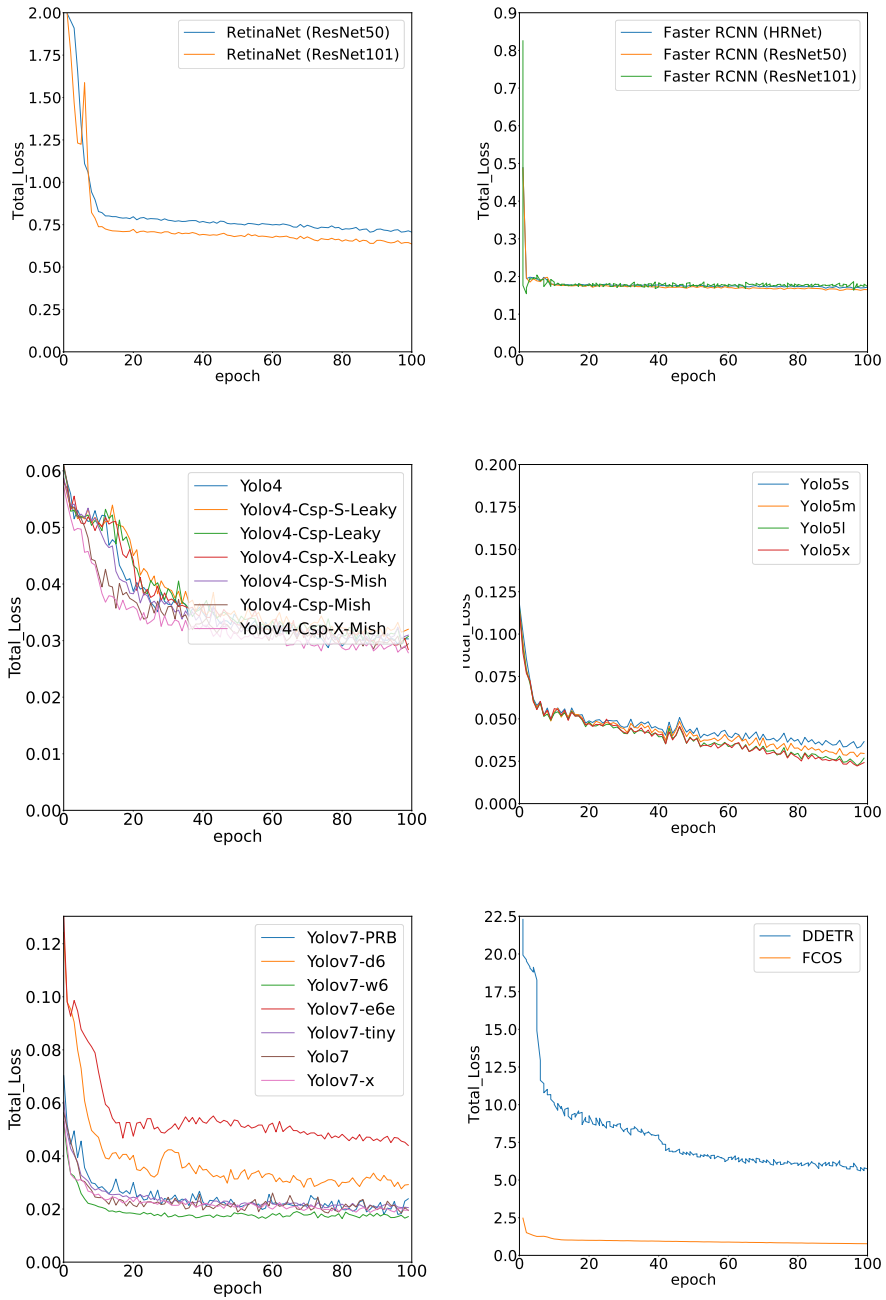


Figure 5: Learning curves of the baselines on our training set.

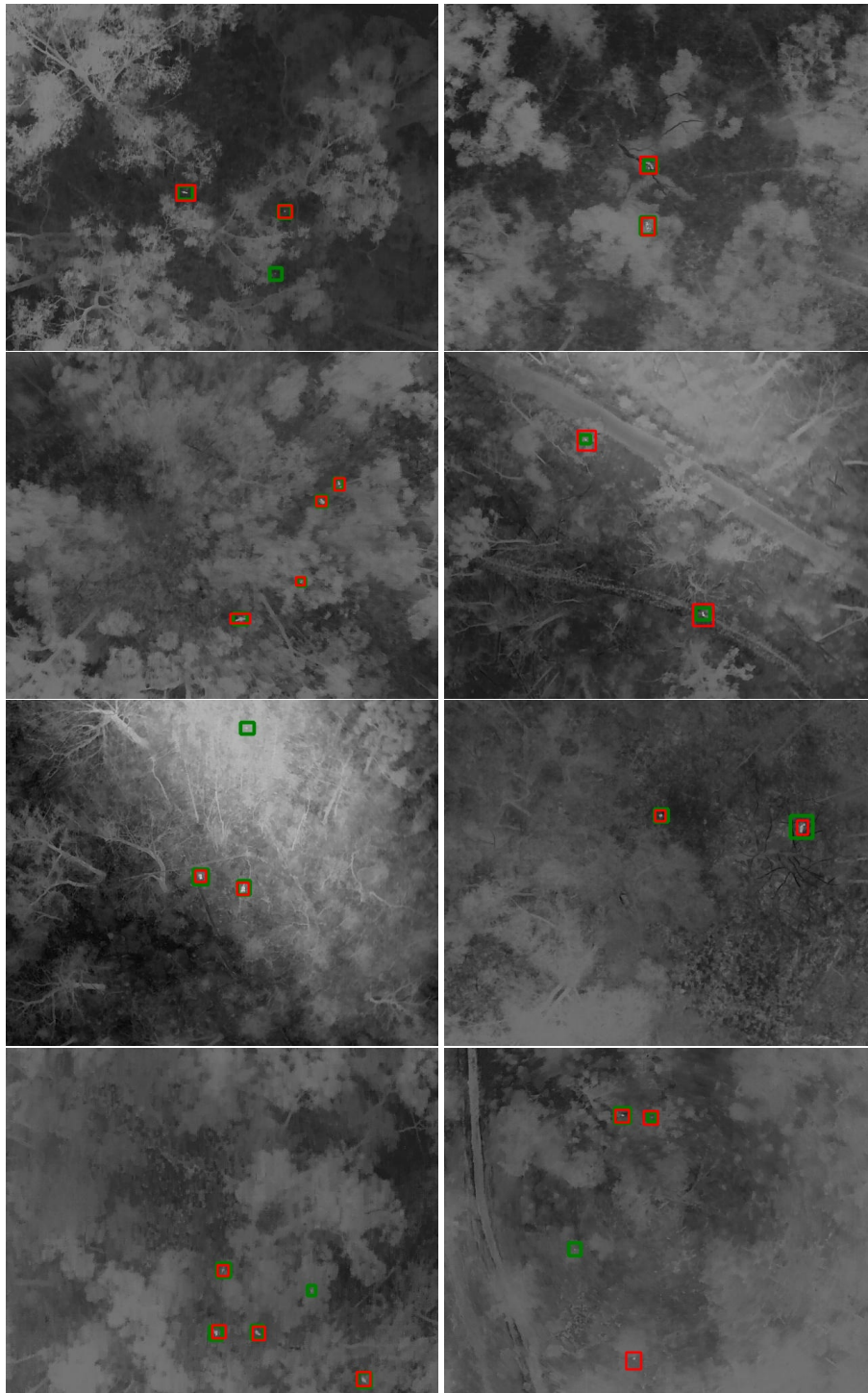


Figure 6: Several detection results of YOLOv5x. Detected objects and annotated objects are presented in green and red.

the ranking of performance in both training and testing of all the baselines remains consistent. Specifically, as shown in Figure 5, YOLOv5 still appears as the best detector during training. It keeps improving during the training (the learning curves slide down continuously) and achieves the best error rate among all the baselines (around 0.025, shown in the vertical axis). In contrast, except for DDETR, other baselines quickly reach their stationary points. For instance, the learning curves of all the variants of Faster RCNN saturate at early epochs (around 10 epochs) with an error rate of 0.2. Likewise, RetinaNet follows this learning trend at early epochs, but then slightly improves. The learning of YOLOv4 and YOLOv7 is less stable, compared with the other baselines, evident by strong fluctuations in their loss curves. Both FCOS and DDETR, despite converging in the learning process, present high error rates. Specifically, the lowest error rates of both FCOS and DDETR are at several magnitude of those of the other baselines. DDETR incurs the highest error rate among all the baselines.

To showcase detection results, we choose YOLOv5x as it is the best detector and illustrate several results of this variant in Figure 6. In general, existing object detectors show their capability of detecting wildlife thermal signatures in realistic conditions. It remains challenging to identify animals presented in small size and in cluttered backgrounds. There requires a more effective design to upsample features in deep architectures to learn features from small-sized objects. We observed that, once detected wildlife species moved, they could be more easily detected by human annotators. This suggests the use of temporal information in improving animal detection.

## 5. Conclusion

This paper presents an empirical review of drone-based wildlife monitoring research since 2018. We provide a concise overview of existing methods regarding hardware specifications and settings, and object detection methods used in animal detection. To benchmark animal detection methods, we collected and annotated a real-world dataset of wildlife thermal signatures in a forested environment, and evaluated state-of-the-art object detectors on our dataset. Experimental results show that YOLOv5 significantly outperforms other baselines in both detection accuracy and computational

speed. The benchmark results also suggest potential research directions including small-sized object detection and using temporal information in detecting animals from drone-derived imagery.

## 6. Acknowledgments

We acknowledge funding from CSIRO under the National Koala Monitoring Program and funding from the Victorian Government’s Department of Environment, Land, Water and Planning to conduct the surveys described in this study. We would also like to thank Desley Whisson for assistance selecting survey sites. We also thank Shelby Ryan for providing flight plans for the surveys described in this study. We also acknowledge Lachlan Clarke and Simon Ruff from the Victorian Government’s Department of Environment, Land, Water and Planning for facilitating access to our survey sites. We also acknowledge Blake Allan for assistance reviewing and facilitating these drone operations as Deakin University’s Chief Remote Pilot.

## References

- [1] S. Legge, D. B. Lindenmayer, N. M. Robinson, B. C. Scheele, D. M. Southwell, B. C. Wintle (Eds.), *Monitoring Threatened Species and Ecological Communities*, CSIRO Publishing, 2018. doi:10.1071/9781486307722.  
URL <https://ebooks.publish.csiro.au/content/9781486307722/9781486307722>
- [2] L. Neal, F. Briggs, R. Raich, X. Z. Fern, Time-frequency segmentation of bird song in noisy acoustic environments, in: *IEEE International Conference on Acoustics, Speech and Signal Processing (ICASSP)*, 2011, pp. 2012–2015.
- [3] D. T. Nguyen, P. O. Ogunbona, W. Li, E. Tasker, J. Yearwood, Detection of ground parrot vocalisation: A multiple instance learning approach, *Journal of the Acoustical Society of America* 142 (3) (2017) 1281–1290.

- [4] Y. Maegawa, Y. Ushigome, M. Suzuki, K. Taguchi, K. Kobayashi, C. Haga, T. Matsui, A new survey method using convolutional neural networks for automatic classification of bird calls, *Ecological Informatics* 61 (2021) 101164.
- [5] T. Denton, S. Wisdom, J. R. Hershey, Improving bird classification with unsupervised sound separation, in: *IEEE International Conference on Acoustics, Speech and Signal Processing (ICASSP)*, 2022, pp. 636–640.
- [6] X. Yu, J. Wang, R. Kays, P. A. Jansen, T. Wang, T. S. Huang, Automated identification of animal species in camera trap images, *EURASIP Journal of Image and Video Processing* 2013 (2013) 52.
- [7] Z. Zhang, Z. He, G. Cao, W. Cao, Animal detection from highly cluttered natural scenes using spatiotemporal object region proposals and patch verification, *IEEE Transactions on Multimedia* 18 (10) (2016) 2079–2092.
- [8] R. Chandrakar, R. Raja, R. Miri, Animal detection based on deep convolutional neural networks with genetic segmentation, *Multimedia Tools and Applications* 81 (2022) 42149–42162.
- [9] Z. Chen, H. Gao, Z. Zhang, H. Zhou, X. Wang, Y. Tia, Underwater salient object detection by combining 2D and 3D visual features, *Neurocomputing* 391 (2020) 249–259.
- [10] N. E. Merencilla, A. S. Alon, G. J. O. Fernando, E. M. Cepe, D. C. Malunao, Shark-EYE: A deep inference convolutional neural network of shark detection for underwater diving surveillance, in: *International Conference on Computational Intelligence and Knowledge Economy (ICCIKE)*, 2021, pp. 384–388.
- [11] X. Wei, L. Yu, S. Tian, P. Feng, X. Ning, Underwater target detection with an attention mechanism and improved scale, *Multimedia Tools and Applications* 80 (25) (2021) 33747–33761.
- [12] Y. Yang, H.-G. Yeh, W. Zhang, C. J. Lee, E. N. Meese, C. G. Lowe, Feature extraction, selection, and K-nearest neighbors algorithm for shark behavior clas-

- sification based on imbalanced dataset, *IEEE Sensors Journal* 21 (5) (2021) 6429–6439.
- [13] C. Yeh, C. Lin, L. Kang, C. Huang, M. Lin, C. Chang, C. Wang, Lightweight deep neural network for joint learning of underwater object detection and color conversion, *IEEE Transactions on Neural Networks Learning Systems* 33 (11) (2022) 6129–6143.
- [14] E. Bennett, H. L. A. Bartlam-Brooks, T. Y. Hubel, A. M. Wilson, Terrestrial mammalian wildlife responses to unmanned aerial systems approaches, *Scientific Reports* 9 (2142) (2019) 1–10.
- [15] E. Corcoran, M. Winsen, A. Sudholz, G. Hamilton, Automated detection of wildlife using drones: Synthesis, opportunities and constraints, *Methods in Ecology and Evolution* 12 (6) (2021) 1103–1114.
- [16] E. Wu, H. Wang, H. Lu, W. Zhu, Y. Jia, L. Wen, C. Choi, H. Guo, B. Li, L. Sun, G. Lei, J. Lei, H. Jian, Unlocking the potential of deep learning for migratory waterbirds monitoring using surveillance video, *Remote Sensing* 14 (3) (2022) 514.
- [17] B. Mirka, D. A. Stow, G. Paulus, A. C. Loerch, L. L. Coulter, L. An, R. L. Lewison, L. S. Pflüger, Evaluation of thermal infrared imaging from uninhabited aerial vehicles for arboreal wildlife surveillance, *Environmental Monitoring and Assessment* 194 (512) (2022) 1–15.
- [18] S. Lee, Y. Song, S. Kil, Feasibility analyses of real-time detection of wildlife using uav-derived thermal and RGB images, *Remote Sensing* 13 (11) (2021) 2169.
- [19] E. Corcoran, S. Denman, J. Hanger, B. Wilson, G. Hamilton, Automated detection of koalas using low-level aerial surveillance and machine learning, *Scientific Reports* 9 (3208) (2019) 1–9.
- [20] S. Hong, Y. Han, S. Kim, A. Lee, G. Kim, Application of deep-learning methods to bird detection using unmanned aerial vehicle imagery, *Sensors* 19 (7) (2019) 1651.

- [21] A. Ulhaq, P. Adams, T. E. Cox, A. Khan, T. Low, M. Paul, Automated detection of animals in low-resolution airborne thermal imagery, *Remote Sensing* 13 (16) (2021) 3276.
- [22] T. Lin, P. Goyal, R. B. Girshick, K. He, P. Dollár, Focal loss for dense object detection, in: *IEEE/CVF International Conference on Computer Vision (ICCV)*, 2017, pp. 2999–3007.
- [23] S. Ren, K. He, R. B. Girshick, J. Sun, Faster R-CNN: towards real-time object detection with region proposal networks, *IEEE Transactions on Pattern Analysis and Machine Intelligence* 39 (6) (2017) 1137–1149.
- [24] J. Redmon, A. Farhadi, YOLO9000: better, faster, stronger, in: *IEEE/CVF Computer Vision and Pattern Recognition (CVPR)*, 2017, pp. 6517–6525.
- [25] Z.-Q. Zhao, P. Zheng, S. tao Xu, X. Wu, Object detection with deep learning: A review, *IEEE Transactions on Neural Networks and Learning Systems* 30 (11) (2019) 3212–3232.
- [26] T. Petso, R. S. J. Jr., D. Mpoeleng, E. Bennitt, W. Mmereki, Automatic animal identification from drone camera based on point pattern analysis of herd behaviour, *Ecological Informatics* 66 (2021) 101485.
- [27] M. Winsen, S. Denman, E. Corcoran, G. Hamilton, Automated detection of koalas with deep learning ensembles, *Remote Sensing* 14 (10) (2022) 2432.
- [28] B. Weinstein, L. Garner, V. Saccomanno, A. Steinkraus, A. Ortega, K. Brush, G. Yenni, A. McKellar, R. Converse, C. Lippitt, A. Wegmann, N. Holmes, A. Edney, T. Hart, M. Jessopp, R. Clarke, D. Marchowski, H. Senyondo, R. Dotson, E. White, P. Frederick, S. Ernest, A general deep learning model for bird detection in high-resolution airborne imagery, *Ecological Applications* 32 (8) (2022) e2694.
- [29] T. Petso, R. S. J. Jr., D. Mpoeleng, Review on methods used for wildlife species and individual identification, *European Journal of Wildlife Research* 68 (3) (2022) 1–18.

- [30] T. E. Cox, R. Matthews, G. Halverson, S. Morris, Hot stuff in the bushes: Thermal imagers and the detection of burrows in vegetated sites, *Ecology and Evolution* 11 (2021) 6406–6414.
- [31] B. Kellenberger, D. Marcos, D. Tuia, Detecting mammals in UAV images: Best practices to address a substantially imbalanced dataset with deep learning, *Remote Sensing of Environment* 216 (2018) 139–153.
- [32] A. Sudholz, S. Denman, A. Pople, M. Brennan, M. Amos, G. Hamilton, A comparison of manual and automated detection of rusa deer (*Rusa timorensis*) from RPAS-derived thermal imagery, *Wildlife Research* 49 (1) (2021) 46–53.
- [33] W. Liu, D. Anguelov, D. Erhan, C. Szegedy, S. Reed, C.-Y. Fu, A. C. Berg, SSD: Single shot multibox detector, in: *European Conference on Computer Vision (ECCV)*, 2016, pp. 21–37.
- [34] J. Dai, Y. Li, K. He, J. Sun, R-FCN: object detection via region-based fully convolutional networks, in: *Conference on Neural Information Processing Systems (NIPS)*, 2016, pp. 379–387.
- [35] K. He, X. Zhang, S. Ren, J. Sun, Deep residual learning for image recognition, in: *IEEE/CVF Computer Vision and Pattern Recognition (CVPR)*, 2016, pp. 770–778.
- [36] J. G. A. Barbedo, L. V. Koenigkan, P. M. Santos, A. R. B. Ribeiro, Counting cattle in UAV images—dealing with clustered animals and animal/background contrast changes, *Sensors* 20 (7) (2020).
- [37] J. Deng, W. Dong, R. Socher, L. Li, K. Li, L. Fei-Fei, Imagenet: A large-scale hierarchical image database, in: *IEEE/CVF Computer Vision and Pattern Recognition (CVPR)*, 2009, pp. 248–255.
- [38] T. Lin, M. Maire, S. J. Belongie, J. Hays, P. Perona, D. Ramanan, P. Dollár, C. L. Zitnick, Microsoft COCO: common objects in context, in: *European Conference on Computer Vision (ECCV)*, 2014, pp. 740–755.

- [39] E. Rublee, V. Rabaud, K. Konolige, G. R. Bradski, ORB: an efficient alternative to SIFT or SURF, in: *IEEE/CVF International Conference on Computer Vision (ICCV)*, 2011, pp. 2564–2571.
- [40] D. G. Lowe, Distinctive image features from scale-invariant keypoints, *International Journal of Computer Vision* 60 (2) (2004) 91–110.
- [41] Z. Tian, C. Shen, H. Chen, T. He, FCOS: fully convolutional one-stage object detection, in: *IEEE/CVF International Conference on Computer Vision (ICCV)*, 2019, pp. 9626–9635.
- [42] X. Zhu, W. Su, L. Lu, B. Li, X. Wang, J. Dai, Deformable DETR: deformable transformers for end-to-end object detection, in: *International Conference on Learning Representation (ICLR)*, 2021, pp. 1–16.
- [43] A. Dosovitskiy, L. Beyer, A. Kolesnikov, D. Weissenborn, X. Zhai, T. Unterthiner, M. Dehghani, M. Minderer, G. Heigold, S. Gelly, J. Uszkoreit, N. Houlsby, An image is worth 16x16 words: Transformers for image recognition at scale, in: *International Conference on Learning Representation (ICLR)*, 2021.
- [44] P. Jiang, D. Ergu, F. Liu, Y. Cai, B. Ma, A review of YOLO algorithm developments, *Procedia Computer Science* 199 (2022) 1066–1073.
- [45] U. Nepal, H. Eslamiat, Comparing YOLOv3, YOLOv4 and YOLOv5 for autonomous landing spot detection in faulty UAVs, *Sensors* 22 (464) (2022) 1–15.
- [46] C. Wang, A. Bochkovskiy, H. M. Liao, YOLOv7: Trainable bag-of-freebies sets new state-of-the-art for real-time object detectors, *CoRR abs/2207.02696* (2022).
- [47] R. Baidya, H. Jeong, YOLOv5 with convmixer prediction heads for precise object detection in drone imagery, *Sensors* 22 (21) (2022) 1–16.
- [48] A. Bochkovskiy, C. Wang, H. M. Liao, YOLOv4: Optimal speed and accuracy of object detection, *CoRR abs/2004.10934* (2020).

- [49] C. Wang, A. Bochkovskiy, H. M. Liao, Scaled-YOLOv4: Scaling cross stage partial network, in: *IEEE/CVF Conference on Computer Vision and Pattern Recognition (CVPR)*, 2021, pp. 13029–13038.
- [50] C.-Y. Wang, H.-Y. Mark Liao, Y.-H. Wu, P.-Y. Chen, J.-W. Hsieh, I.-H. Yeh, CSPNet: A new backbone that can enhance learning capability of CNN, in: *IEEE/CVF Conference on Computer Vision and Pattern Recognition Workshops (CVPRW)*, 2020, pp. 390–391.
- [51] P. Chen, M. Chang, J. Hsieh, Y. Chen, Parallel residual bi-fusion feature pyramid network for accurate single-shot object detection, *IEEE Transactions on Image Processing* 30 (2021) 9099–9111.
- [52] K. Sun, B. Xiao, D. Liu, J. Wang, Deep high-resolution representation learning for human pose estimation, in: *IEEE/CVF Computer Vision and Pattern Recognition (CVPR)*, 2019, pp. 5686–5696.